

Rose-Hulman Institute of Technology Rose-Hulman Scholar

Rose-Hulman Undergraduate Research Publications

6-10-2015

Spectrally-resolved Imaging of the Transverse Modes in Multimode VCSELs

Stephan A. Misak

Rose-Hulman Institute of Technology

Dan G. Dugmore

Rose-Hulman Institute of Technology

Kirsten A. Middleton

Rose-Hulman Institute of Technology

Evan R. Hale


Rose-Hulman Institute of Technology

Kelly R. Farner

Rose-Hulman Institute of Technology

See next page for additional authors

Follow this and additional works at: http://scholar.rose-hulman.edu/undergrad_research_pubs

 Part of the [Computer Sciences Commons](#), [Engineering Physics Commons](#), [Life Sciences Commons](#), and the [Semiconductor and Optical Materials Commons](#)

Recommended Citation

Misak, Stephan A.; Dugmore, Dan G.; Middleton, Kirsten A.; Hale, Evan R.; Farner, Kelly R.; Choquette, Kent D.; and Leisher, Paul O., "Spectrally-resolved Imaging of the Transverse Modes in Multimode VCSELs" (2015). *Rose-Hulman Undergraduate Research Publications*. 8.

http://scholar.rose-hulman.edu/undergrad_research_pubs/8

This Article is brought to you for free and open access by Rose-Hulman Scholar. It has been accepted for inclusion in Rose-Hulman Undergraduate Research Publications by an authorized administrator of Rose-Hulman Scholar. For more information, please contact weir1@rose-hulman.edu.

Authors

Stephan A. Misak, Dan G. Dugmore, Kirsten A. Middleton, Evan R. Hale, Kelly R. Farner, Kent D. Choquette, and Paul O. Leisher

Spectrally-resolved Imaging of the Transverse Modes in Multimode VCSELs

Stephen M. Misak¹, Dan G. Dugmore¹, Kirsten A. Middleton¹, Evan R. Hale¹,
Kelly R. Farner¹, Kent D. Choquette², and Paul O. Leisher^{1,*}

¹ Rose-Hulman Institute of Technology, 5500 Wabash Ave., Terre Haute, IN 47803, USA

² University of Illinois at Urbana-Champaign, 208 N. Wright St., Urbana, IL 61801, USA

ABSTRACT

Vertical-cavity surface-emitting lasers (VCSELs) enable a range of applications such as data transmission, trace sensing, atomic clocks, and optical mice. For many of these applications, the output power and beam quality are both critical (i.e. high output power with good beam quality is desired). Multi-mode VCSELs offer much higher power than single-mode devices, but this comes at the expense of lower beam quality. Directly observing the resolved mode structure of multi-mode VCSELs would enable engineers to better understand the underlying physics and help them to develop multi-mode devices with improved beam quality. In this work, a low-cost, high-resolution (<3 pm) Echelle grating spectrometer system is used to map the two-dimensional VCSEL near-field emission profile. The system spectrally disperses the VCSEL beam and images it with high magnification onto a CMOS camera. The narrow spectral content of each LP mode allows direct observation of the modal content of the VCSEL.

Keywords: multi-mode VCSEL, Echelle grating spectrometer, LP mode

1. MOTIVATION

Semiconductor lasers emit light perpendicular to their surface while VCSELs are built with layers of distributed Bragg reflectors (DBRs) and a central active region containing multiple quantum wells. The photons are emitted by pumping current into a ring electrode in the active region between oppositely doped DBR layers, forming a p-n junction diode. While the range of possible emission wavelengths is limited by the materials used in the VCSEL design, the exact lasing frequency is selected by the design of the resonant cavity (in all three dimensions). VCSELs designed with a larger mode areas result in higher power, however beam quality is degraded due to multi-mode operation in both the lateral and vertical direction.

Directly observing the resolved 2D mode structure of multi-mode VCSELs would help engineers develop a better understanding of the underlying physics in order to design multi-mode devices with improved beam quality. The typical near-field emission profile of a VCSEL is a 2D image which shows the overall intensity pattern arising from the interaction of all lasing modes, each operating at a slightly different wavelength. In a manner similar to the 1D case for edge-emitting lasers, the observed near-field mode profile is simply the summation of the individual eigenmodes of the 2D VCSEL cavity.

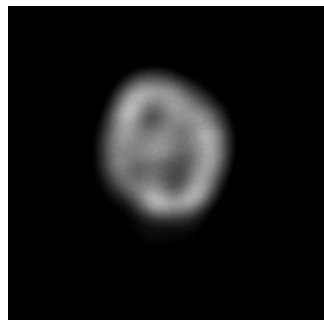


Figure 1. Example near-field image profile of a multimode VCSEL

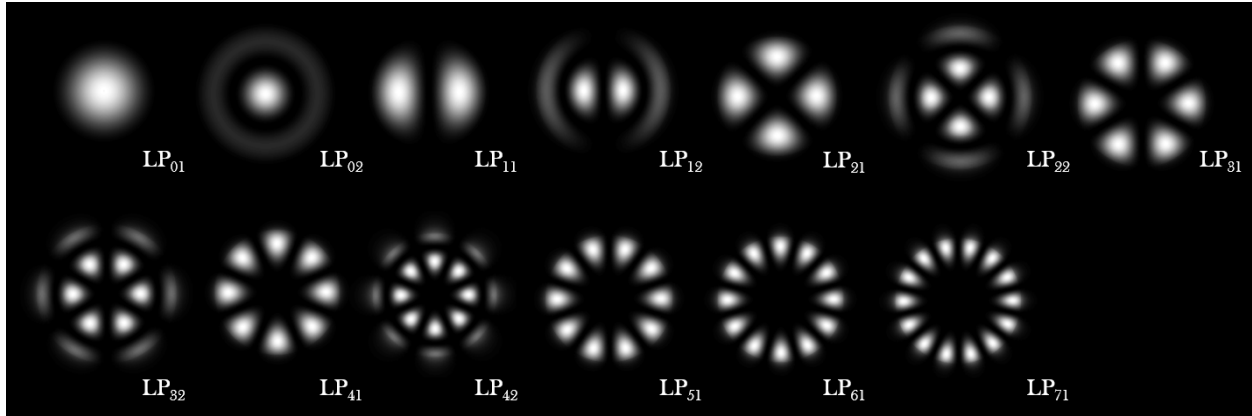


Figure 2. Theoretical images of the separated VCSEL modes.

Further research with VCSELs is advantageous because of their benefits over edge-emitting lasers. VCSEL's vertical wafer design makes them more efficient and inexpensive. Their ability to be integrated into an array also presents a key advantage. With applications in optical communications, interconnects, neural networks, and signal processing, developing a greater understanding of the multi-mode VCSELs can lead to improvements in several industries. Multi-mode VCSELs are typically avoided because of mode competition [2]. With more knowledge from research, the instability in multi-mode VCSELs can be reduced, improving beam quality and increasing the possibilities for VCSEL technology.

* pleisher@ieee.org; Tel: (812) 877-8824

2. EXPERIMENT

Imaging the transverse modes of a multi-mode VCSEL was accomplished using a custom benchtop high resolution Echelle spectrometer. Figure 3 illustrates the design. The beam is magnified, collimated, dispersed, and reimaged. A 13.86 mm focal length asphere and a 200 mm focal length spherical lens are used to magnify the VCSEL beam and image it at the diffraction limit. After passing through a periscope, the beam is collimated with a 500 mm focal length lens both before and after diffracting off the grating. An Echelle grating with 79 grooves/mm and a 75° blaze angle is used in the Littrow configuration to disperse the VCSEL near-field and resolve the mode content. The beam splitter is used to redirect the dispersed beam to the CMOS camera. The slit which is normally at the image plane was removed in order to view the entire 2D mode structure of the VCSEL. A single pass off the grating was used when imaging the modes, but a mirror could be used to improve the resolution by double passing the grating. For this experiment, a double pass was not needed to acquire the images of the VCSEL modes. A polarizer and a second magnifying lens with $f=50\text{mm}$ were used to observe the effect of polarization and to improve image size.

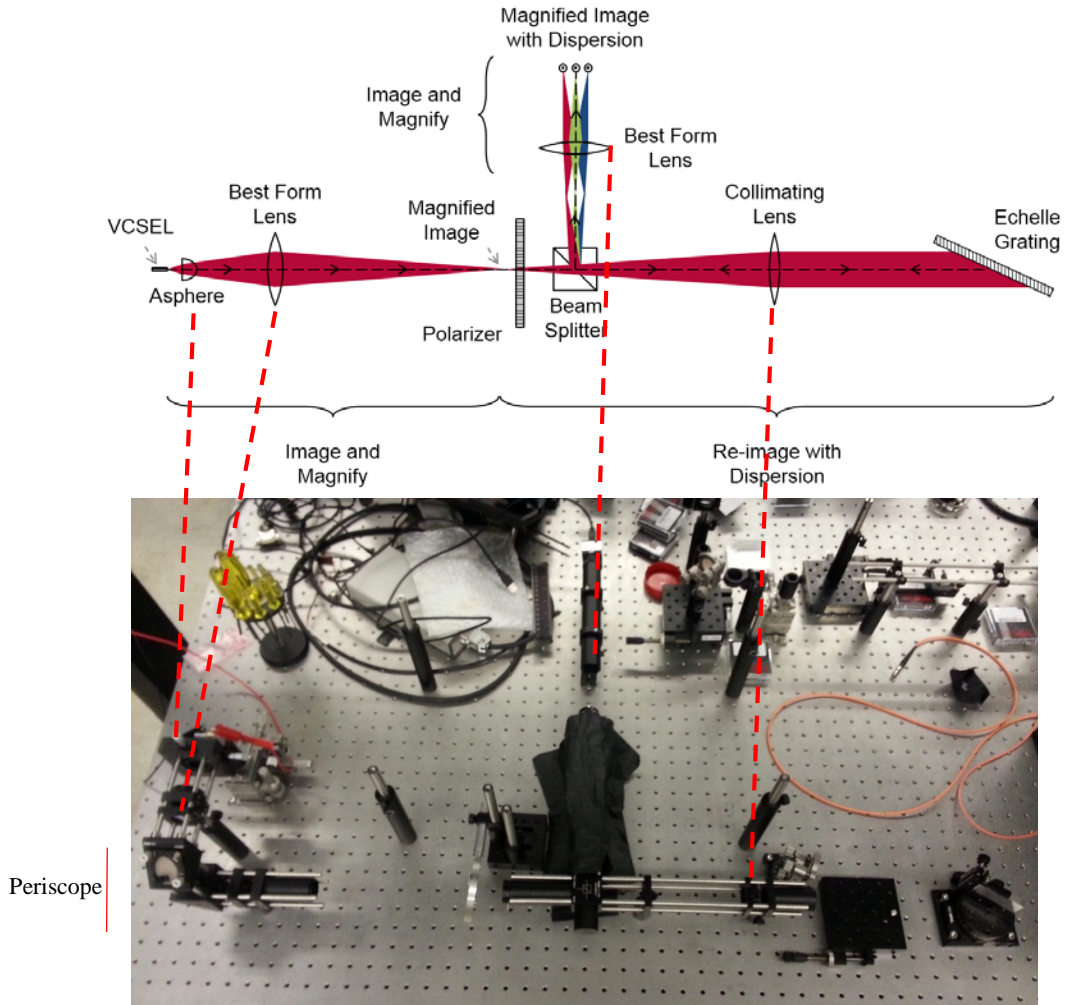


Figure 3. (Top) Modified Spectrometer Diagram. (Bottom) Modified Spectrometer Overview.

The VCSEL used for all of the tests was a packaged multi-mode laser diode. It was manufactured with a $15.1 \mu\text{m}$ oxide aperture, and it features a flat window and monitor photodiode. Typical power and wavelength were rated at 1.85mW ($I_f = 8\text{mA}@RT$) and 845 nm accordingly. The measured spectrum and output power data are as shown in Figure 4. The optical power was measured with a switchable gain, amplified silicon detector. The spectrum data was gathered at a resolution of 0.02 nm .

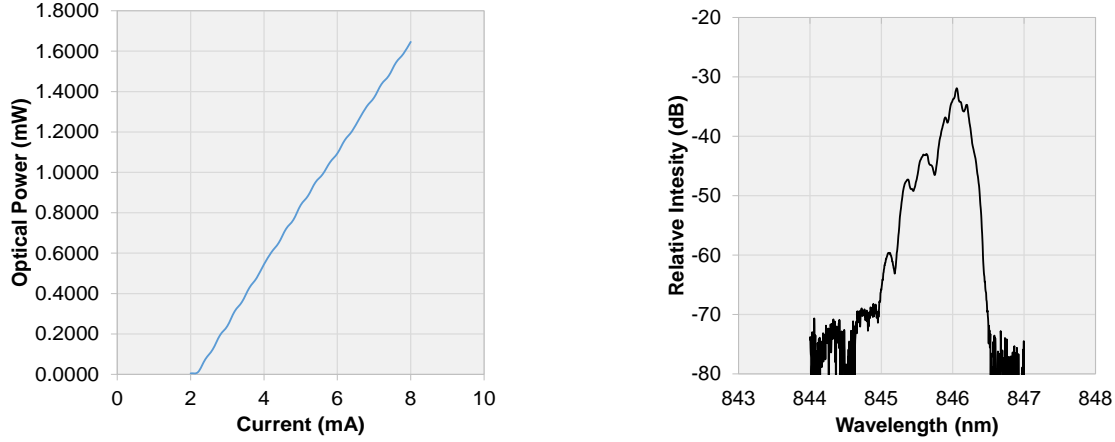


Figure 4. (Left) Optical output power vs. input current. (Right) Logarithmic scale spectrum at 8 mA.

Theoretical calculations were also made in order to compare the experimental data with an expected outcome. MATLAB software was used to generate the theoretical plots based on the equations governing the LP modes of guided waves. The software used to plot the theoretical VCSEL mode structure was adapted from [6]. The X parameter limit was defined using the V parameter, defined in Eq. (2-1) [3, 4].

$$V = 2\pi \frac{a}{\lambda_0} NA, \quad NA = \sqrt{n_1^2 - n_2^2} \quad (2-1)$$

The LHS and RHS of the characteristic equation (2-2) were plotted to find the values of X_{lm} where the plots intersect and a mode exists [3, 4]. After solving for the values of the X parameter for each of the modes, the expressions (2-3) are used to plot the intensity line profile of each mode radially outward. The program uses the angular index of the mode to create an angular profile of the mode. The program uses a function [5] to transform the cylindrical coordinates into Cartesian so that they can be plotted as a surface.

$$X \frac{J_{l\pm 1}(X)}{J_l(X)} = \pm Y \frac{K_{l\pm 1}(Y)}{K_l(Y)}, \quad Y = \sqrt{V^2 - X^2} \quad (2-2)$$

$$\frac{J_l(X_{lm} \frac{r}{a})}{J_l(X_{lm})}, \quad \frac{K_l(Y_{lm} \frac{r}{a})}{K_l(Y_{lm})} \quad (2-3)$$

In order to create a theoretical mode structure for the VCSEL which corresponded to the experimental setup, the modes needed to be spaced apart the correct distance. Using the X parameter to calculate the value of β_{lm} with Eq. (2-4), the wavelength spacing was found by finding the corresponding λ for each β_{lm} value with Eq. (2-5) [3, 4] and taking the difference.

$$\beta_{lm} = \sqrt{n_1^2 k_0^2 - \frac{X_{lm}^2}{a^2}} \quad (2-4)$$

$$\beta = k_0 n, \quad k_0 = \frac{2\pi}{\lambda_0} \quad (2-5)$$

In order to find the physical distance between the modes in the final image, the angular spread from the grating was used with a right triangle approximation. The correct diffraction order was found using the Littrow configuration of the grating equation (2-6). The angular spread was calculated by taking the difference between the β angles of the highest and the lowest wavelength (846nm, 845 nm). To calculate the physical height, the boundary rays were approximated to form a right triangle after passing through the collimating lens. Using the angular spread and the focal

length of the lens, the height of the image was approximated with Eq. (2-7). The ratio between the change in wavelength and the image height was used to correctly space the modes in the theoretical image, Figure 6.

$$\sin(\alpha) + \sin(\beta) = \frac{m\lambda}{d}, \sin(\theta) = \frac{m\lambda}{2d} \quad (2-6)$$

$$h = f \cdot \tan(\Delta\theta) \quad (2-7)$$

3. RESULTS AND DISCUSSION

Several different images were constructed by compiling raw image data. Figure 5 illustrates a comparison between the theoretical LP modes and the VCSEL modes. To acquire high quality images in Figure 5, several images from different currents were combined. The polarizer was adjusted to reduce inference from mode overlap while changing the exposure time to adjust to the intensity. Figure 6 is a complete profile of the beam at several different currents. For each current, several images were taken and combined to avoid over exposure. The theoretical mode structure is shown for comparison; its development is as described in the previous section. The LP₀₁ and LP₁₁ modes appear unstable as the current is changed, having high intensity at certain currents while not visible at others. Both polarization states are lasing as evidenced by the overlap of the two LP₁₁ orientations.

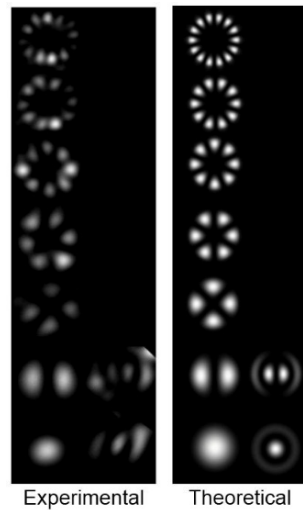


Figure 5. Individual mode comparison to theoretical modes.

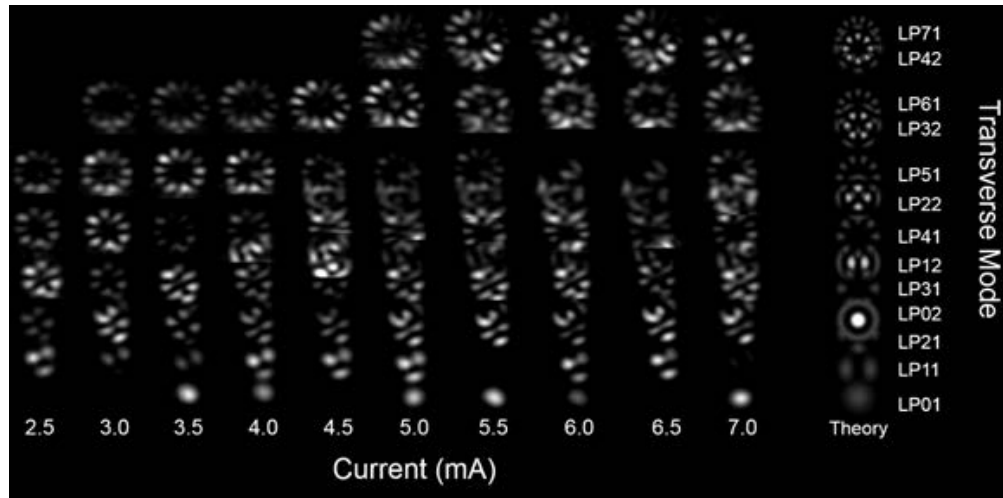


Figure 6. Complete VCSEL mode structure with increasing current compared to theoretical mode structure

To further investigate the polarization of the modes, images of the beam were taken with the polarizer in different orientations. Figure 4(a) and (b) confirm that both orientations of the LP_{11} are overlapping by isolating each orientation using the polarizer. An unexpected effect of polarization was observed with the LP_{71} mode. The overlapping mode is lasing in a different polarization state. Different polarization states between modes were not otherwise observed.

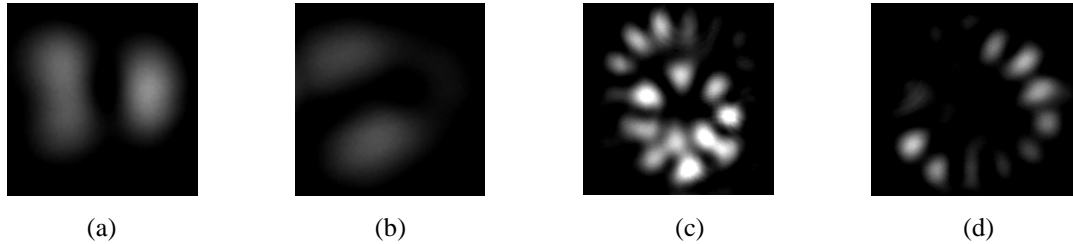


Figure 7. (a) LP_{11e} mode. (b) LP_{11o} mode. (c) LP_{71} mode with overlapping mode in a different polarization state (LP_{42} according to theory). (d) LP_{71} mode with polarizer blocking the light from the overlapping mode.

The VCSEL near-field was also imaged with a single exposure for each current to show the trend as the higher index modes increased in intensity. The instability of the LP_{01} and LP_{11} modes is again evident as the relative intensity greatly varies between currents. Instability in relative intensity is evident to some degree in all the modes. The LP_{31} and the LP_{12} modes exhibit a general increasing trend in relative intensity. The outer edges of the LP_{22} mode are barely visible at 8.0mA, showing an increase in the brightness of the mode at higher current.

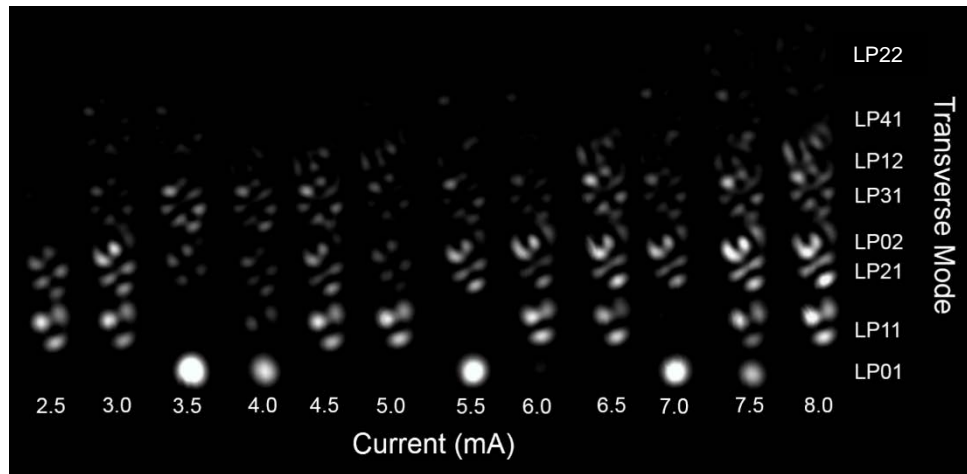


Figure 8. VCSEL near-field with increasing current. One image is take at each value of current.

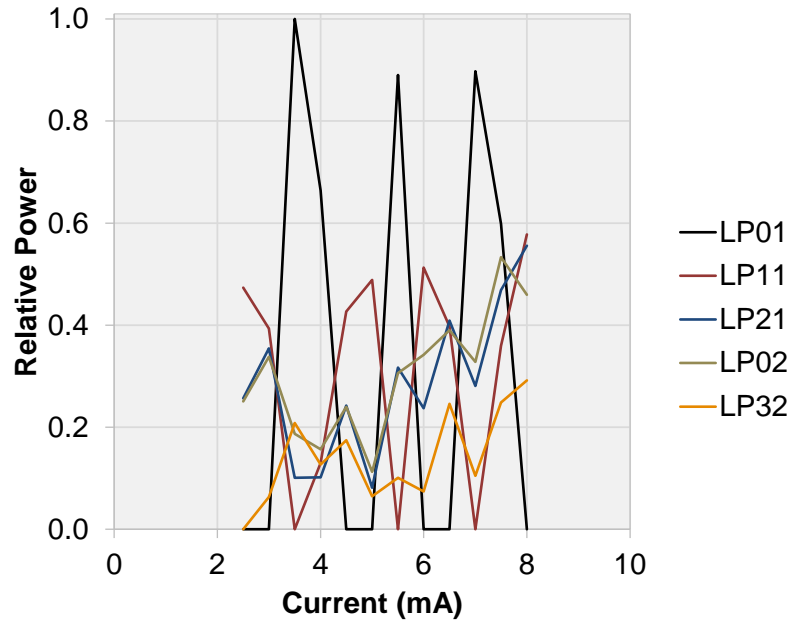


Figure 9. Relative Power of LP modes based on Figure 8

4. CONCLUSION

The goal of this work was to adapt the spectrometer setup to image the transverse modes of a multi-mode VCSEL. The spectrometer was modified by removing the slit while adding a new mount, magnifying lens, and polarizer. With the modifications, the VCSEL transverse modes were able to be imaged due to their narrow frequency spread. The mode structure for the VCSEL closely corresponded to the expected structure for a circular aperture.

REFERENCES

- [1] P. Crump, S. Boldicke, C. Shultz, H. Ekhteraei, H. Wenzel, and G. Erbert, "Experimental and theoretical analysis of the dominant lateral waveguiding mechanism in 975 nm high power broad area diode lasers," *IOP Semicond. Sci. Technol.*, vol. 27, no. 045001, 2012.
- [2] Transverse mode characteristics of vertical cavity surface-emitting lasers. Chang-Hasnain, C. J. and Orenstein, M. and Von Lehmen, A. and Florez, L. T. and Harbison, J. P. and Stoffel, N. G., *Applied Physics Letters*, 57, 218-220 (1990). 11 July 2011.
- [3] Saleh, Bahaa E. A., and Malvin C. Teich. "Fiber Optics." *Fundamentals of Photonics*. 2nd ed. N.p.: Wiley, 2007. 327-59. *Signal Lake*. Signal Lake Management. Web. 14 Aug. 2014.
- [4] Saleh, Bahaa E. A., and Malvin Carl. Teich. *Fundamentals of Photonics*. New York: Wiley, 1991. Print.
- [5] J M De Freitas. POLAR3D: A 3-Dimensional Polar Plot Function in Matlab. QinetiQ Ltd, Winfrith Technology Centre, Winfrith, Dorchester DT2 8XJ. UK. 2 June 2005.
- [6] Bojor, Lucian. *Fiber Modes*. Computer software. *Matlab Central*. The MathWorks, Inc., 29 Nov. 2005. Web. 14 Aug. 2014.